Dyes and Pigments 99 (2013) 599–606

Contents lists available at SciVerse ScienceDirect

Dyes and Pigments

journal homepage: www.elsevier.com/locate/dyepig

Dual-channel anchorable organic dye with triphenylamine-based core bridge unit for dye-sensitized solar cells

Kang Deuk Seo [a], Ban Seok You [a], In Tack Choi [a], Myung Jong Ju [a], Mi You [b], Hong Seok Kang [b], Hwan Kyu Kim [a,*]

[a] Global GET-Future Laboratory, Department of Advanced Materials Chemistry, Korea University, Sejong 339-700, South Korea
[b] Department of Nano & Advanced Materials, College of Engineering, Jeonju University, Chonju, Chonbuk 560-759, South Korea

ARTICLE INFO

Article history:
Received 18 May 2013
Received in revised form
12 June 2013
Accepted 14 June 2013
Available online 2 July 2013

Keywords:
Dye-sensitized solar cell
Dual-channel
Core bridge donor
Triphenylamine
Dye aggregation
Coadsorbent

ABSTRACT

Dual-channel (DC) anchorable organic dye based on an acceptor–π–donor-core bridge donor–donor–π-acceptor structural motif, was synthesized and used as sensitizer for dye sensitized solar cells (DSSCs). DC dye linked the two donors using a core bridge donor such as triphenylamine unit, which makes two channels maintaining a particular distance (>4 Å). The inter-planar DC5 exhibited dye aggregation and charge recombination due to strongly intermolecular π–π stacking between the channels of DC dyes adsorbed on the TiO_2 surface. As a result, a solar cell based on DC5 with a hole conductor coadsorbent of HC-A1 showed better photovoltaic performance with a J_{sc} of 8.90 mA cm^{-2}, a V_{oc} of 0.70 V, and an *FF* of 0.77, corresponding to an overall conversion efficiency (η) of 4.80%.

Published by Elsevier Ltd.

1. Introduction

Dye-sensitized solar cells (DSSCs) are promising hybrid/organic photovoltaic devices for high efficiency, low cost solar energy conversion [1–4]. In these cells, the sensitizer is one of the key components for high power-conversion efficiency. Recently, interest in metal-free organic dyes as an alternative to noble metal complexes has increased due to their many advantages, such as the diversity of molecular structures, high molar extinction coefficients, simple synthesis, as well as low cost and negligible environmental issues [5–8]. By employing a combination of a zinc porphyrin dye (YD2-*o*-C8) and an organic dye (Y123) in conjunction with a tris(2,2′-bipyridine) cobalt(II/III) redox couple, Grätzel et al. reported a 12.3% efficiency DSSCs [9]. Many organic dyes based on the donor–(π-spacer)–acceptor (D–π–A) system, exhibiting relatively high DSSCs performance, have so far been designed and developed. A single D–π–A sensitizer having a rod-like configuration may cause undesirable dye aggregation and charge recombination [10–13]. The intermolecular π-π stacking of dye molecules can lead to self-quenching of excited states and hence inefficient electron injection [14]. A common structural strategy for suppression of dye aggregation is the introduction of a bulky group to the donor part [15,16]. Another unique approach is bridging of two chromophores into a spiro configuration similar to Ru-sensitizers [17]. To enhance optical density and binding strength of the dye onto TiO_2, of particular interest is the synthesis of a dianchoring dye, which has been found to enhance the photocurrent due to the extended π-conjugated framework and higher molar extinction coefficient. Several dianchoring organic dyes have been synthesized for use in DSSCs, and have demonstrated better cell performance than single D–π–A sensitizers with an improved photoresponse, photocurrent and stability [18–22].

In this study, we present an extension of dianchoring organic sensitizer, with the aim of further expanding the possibility of improving the optical and energetic properties of the sensitizers. The new approach, based on the acceptor–π–donor-core bridge donor–donor–π-acceptor structural motif, includes the use of two donors, two acceptors and a core bridge donor as a spacer. We have adapted diphenylamine as a donor group by using a core bridge donor such as triphenylamine units. The dual-channel anchorable organic dye which contained two separate light-harvesting units and two anchoring group in one molecule has higher molar extinction coefficient

* Corresponding author. Tel.: +82 44 860 1493; fax: +82 44 867 5396.
E-mail addresses: hsk@jj.ac.kr (H.S. Kang), hkk777@korea.ac.kr (H.K. Kim).

0143-7208/$ – see front matter Published by Elsevier Ltd.
http://dx.doi.org/10.1016/j.dyepig.2013.06.014

and increases the binding strength of dye on TiO_2 film. Also, the hexyloxy group was introduced into the triphenylamine moiety for increase the electron-donating ability and decrease the dye aggregation, charge recombination. For comparison, the photophysical properties and photovoltaic performances of a single D–π–A structured D21L6 were also studied (see Scheme 1, Fig. 1, Tables 1 and 2).

2. Experimental

2.1. Materials

All reactions were carried out under a nitrogen atmosphere. Solvents were distilled from appropriate reagents. All reagents were purchased from Aldrich. (5′-(1,3-Dioxolan-2-yl)-2,2′-bithiophen-5-yl)tributyl stannane [23] and D21L6 [24] were synthesized by following the same procedures as described previously.

2.2. Measurements

^{1}H NMR and ^{13}C NMR spectra were recorded at room temperature with Varian Oxford 300 spectrometers and chemical shifts were reported in ppm units with tetramethylsilane as the internal standard. FTIR spectra were taken on a JASCO, 4200 + ATR Pro-450-S spectrophotometer. UV–visible absorption spectra were obtained in THF on a Shimadzu UV-2401PC spectrophotometer. Cyclic voltammetry was carried out with a Versa STAT3 (AMETEK). A three-electrode system was used and consisted of a reference electrode (Ag/AgCl), a working electrode, and a platinum wire electrode. The

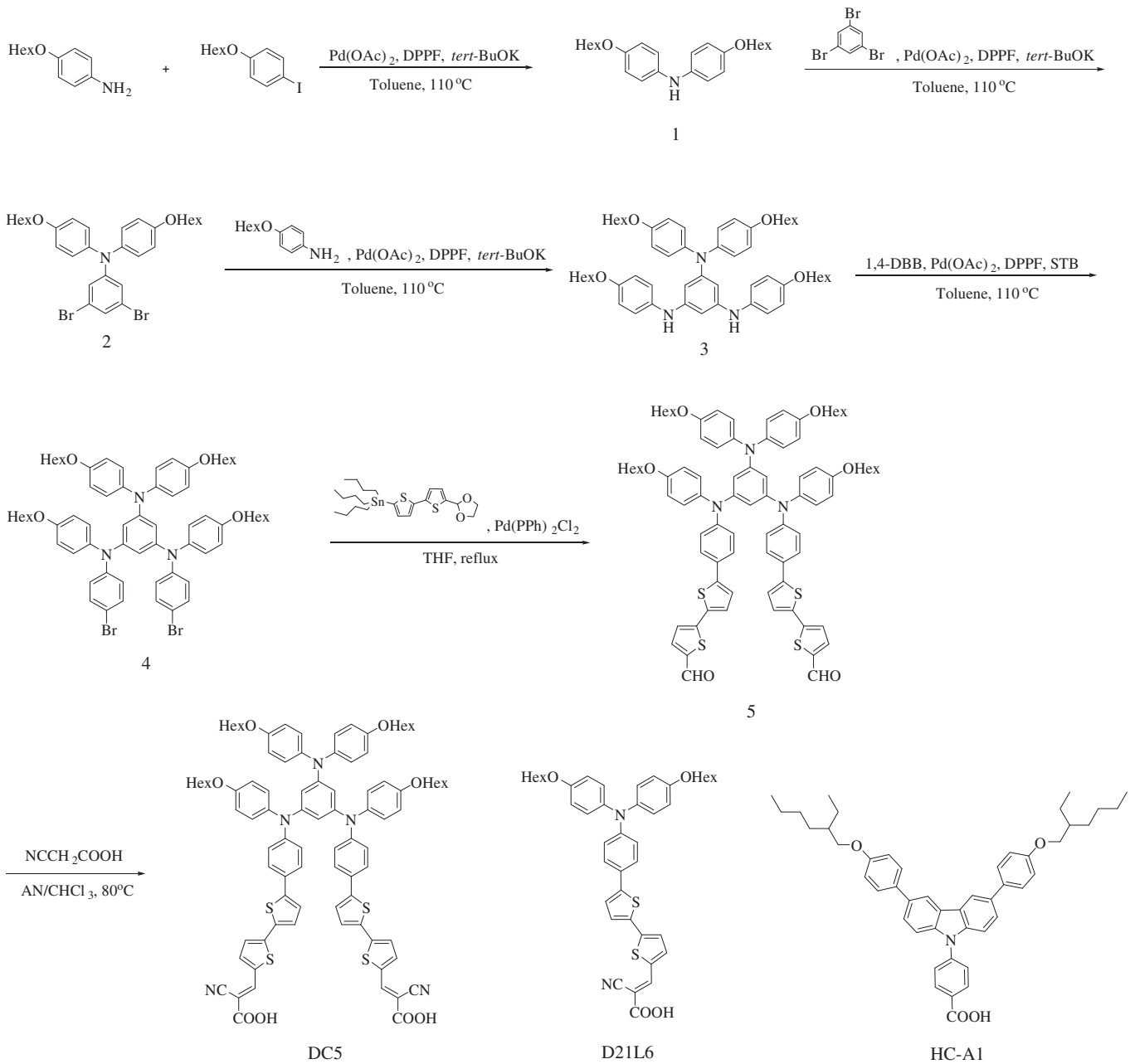

Scheme 1. Chemical structures and synthesis of DC5 dye.

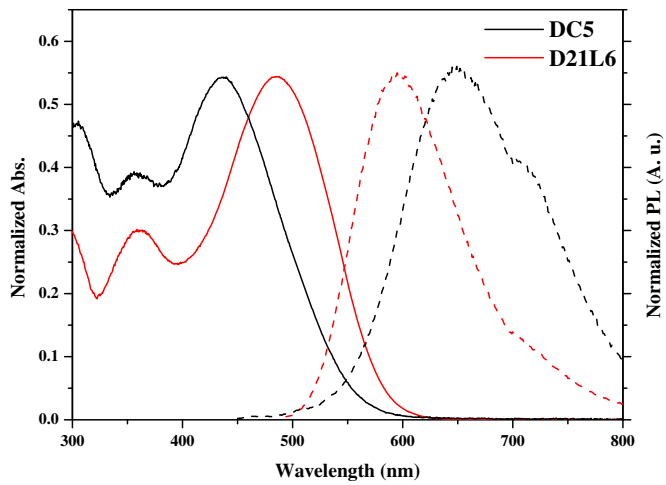

Fig. 1. Absorption and emission spectra of DC5 dye with the concentration of 2×10^{-5} M in THF.

redox potential of dyes on TiO_2 was measured in CH_3CN with 0.1 M $TBAPF_6$ with a scan rate between 50 mV s^{-1}.

2.3. Density functional theory (DFT)/time-dependent DFT (TDDFT) calculations

Structural optimization of dual-channel (DC) dye was done with a PBE exchange-correlation function using the Vienna ab initio simulation package (VASP) [25,26]. We used 400 eV as the cut-off energy, and the conjugate gradient method was employed to optimize the geometry until the force exerted on an atom was less than 0.03 eV/Å. The size of the super cell was maintained large enough to guarantee the closest distance between atoms belonging to the neighboring cells was larger than 16 Å. More precisely, structure optimizations were done for two configurations for the dye, i.e., *cis* and *trans* configurations. In order to calculate the absorption spectra, we performed the TD-DFT calculations for more stable one between the two configurations. Calculations were done in the gas phase using the 6-31G(d,p) basis set in GAUSSIAN03 program [27]. We focused on transitions occurring in the range of 350–800 nm, specifically those whose oscillation strengths were greater than 0.1. In order to treat the low wavelength excitations correctly around 350 nm, we made extensive calculations up to 100 singlet → singlet transitions.

2.4. Synthesis

2.4.1. Bis-(4-(hexyloxy) phenyl) amine (1)

A mixture of 4-(hexyloxy)benzenamine (3.00 g, 9.86 mmol), 1-(hexyloxy)-4-iodobenzene (2.10 g, 10.9 mmol), $Pd(OAc)_2$ (0.10 g, 0.45 mmol), bis(diphenylphosphinyl)ferrocene (DPPF) (0.52 g, 0.94 mmol), and sodium *tert*-butoxide (2.84 g, 29.6 mmol) was heated in dry toluene at 110 °C under an inert N_2 atmosphere. After 12 h, the crude reaction mixture was treated with a saturated ammonium chloride solution and extracted with dichloromethane. The organic phase was washed with brine, dried over $MgSO_4$, and the solvent was evaporated under vacuum. The crude product was purified by column chromatography (silica gel, MC–hexane 2:1) to give 1.91 g (52%) of compound 1. ^{1}H NMR (300 MHz, DMSO-d_6) compound: δ 0.85 (t, 6H), 1.27–1.42 (m, 12H), 1.64–1.69 (m, 4H), 3.84 (t, 4H), 6.77 (d, 4H), 6.87 (d, 4H), 7.48(s, 1H); ^{13}C NMR (300 MHz, DMSO-d_6) δ: 4.24, 12.4, 15.6, 19.1, 21.3, 58.0, 105.5, 108.2, 128.2, 142.4.

Table 1
Optical properties of DC5 dye.

Dye	Absorption λ_{max}/(nm)[a], ε (M^{-1} cm^{-1})	Emission (λ_{max}/nm)	E_{ox}[b]/V (vs. NHE)	E_{0-0}[c]/V	E_{LUMO}[d]/V (vs. NHE)
DC5	440 (41700)	645	0.94	2.26	−1.32
D12L6	486 (27700)	597	0.96	2.27	−1.31

[a] Absorption and emission spectra were measured in THF.
[b] Oxidation potentials of dyes on TiO_2 were measured in CH_3CN with 0.1 M $TBAPF_6$ with a scan rate of 50 mV s^{-1} (vs. NHE).
[c] E_{0-0} was determined from the intersection of absorption and emission spectra in $CHCl_3$/MeOH.
[d] LUMO was calculated by $E_{ox} - E_{0-0}$.

Table 2
Dye-sensitized solar cell performance data of the DC5 dye.

Dye	Coabs.	$\Gamma/10^{-7}$ (mol cm^{-2})	J_{sc} (mA/cm^2)	V_{oc} (V)	*FF*	η (%)
DC5	–	1.72	1.34	0.45	0.76	0.46
	DCA 40 mM	1.51	5.70	0.54	0.78	2.41
	HC-A1 1 mM	1.24	8.92	0.69	0.77	4.78
D21L6	DCA 40 mM	1.92	13.8	0.67	0.72	6.67
N719	–		16.7	0.71	0.73	8.64

TiO_2 thickness 13,14 + 2,sc,$TiCl_4$; electrolyte condition 0.6 M DMPII, 0.5 M LiI, 0.05 M I_2, 0.5 M TBP in an acetonitrile solution; dye was dissolved in THF/MeOH.

2.4.2. 3,5-Dibromo-N,N-bis(4-(hexyloxy)phenyl)benzenamine (2)

A mixture of compound 1 (1.50 g, 4.06 mmol), 1,3,5-tribromobenzene (3.83 g, 12.2 mmol), $Pd(OAc)_2$ (0.05 g, 0.22 mmol), DPPF (0.22 g, 0.40 mmol), and sodium *tert*-butoxide (1.17 g, 12.2 mmol) were heated in dry toluene at 110 °C under an inert N_2 atmosphere. After 12 h, the crude reaction mixture was treated with a saturated ammonium chloride solution and extracted with dichloromethane. The organic phase was washed with brine, dried over $MgSO_4$, and the solvent was evaporated under vacuum. The crude product was purified by column chromatography (silica gel, MC–hexane 1:8) to give 1.65 g (67%) of compound 2. ^{1}H NMR (300 MHz, $CDCl_3$) δ: 0.89 (t, 6H), 1.34–1.55 (m, 12H), 1.73–1.80 (m, 4H), 3.91 (t, 4H), 6.83 (m, 6H), 7.04 (m, 5H); ^{13}C NMR (300 MHz, $CDCl_3$) δ: 14.2, 22.8, 25.9, 29.5, 31.8, 68.4, 115.7, 120.0, 123.1, 124.5, 139.1, 151.3, 156.5.

2.4.3. N^1,N^1,N^3,N^5-Tetrakis(4-(hexyloxy)phenyl)benzene-1,3,5-triamine (3)

A mixture of compound 2 (1.50 g, 2.49 mmol), 4-(hexyloxy) benzenamine (1.05 g, 5.43 mmol), $Pd(OAc)_2$ (0.03 g, 0.13 mmol), DPPF (0.14 g, 0.25 mmol), and sodium *tert*-butoxide (0.72 g, 7.49 mmol) were heated in dry toluene at 110 °C under an inert N_2 atmosphere. After 12 h, the crude reaction mixture was treated with a saturated ammonium chloride solution and extracted with dichloromethane. The organic phase was washed with brine, dried over $MgSO_4$, and the solvent was evaporated under vacuum. The crude product was purified by column chromatography (silica gel, MC–hexane 2:1) to give 1.10 g (53%) of compound 3. ^{1}H NMR (300 MHz, $CDCl_3$) δ: 0.89 (m, 12H), 1.34–1.45 (m, 24H), 1.70–1.81 (m, 8H), 3.85–3.94 (m, 8H), 6.30 (s, 2H), 5.97 (s, 2H), 6.06 (s, 1H), 6.71(t, 8H), 6.93 (d, 4H), 7.04 (d, 4H); ^{13}C NMR (300 MHz, $CDCl_3$) δ: 14.2, 22.8, 25.9, 29.5, 31.8, 68.4, 95.5, 100.7, 115.1, 121.7, 126.8, 135.7, 140.9, 146.3, 150.8, 154.5, 155.3.

2.4.4. N^1,N^3-Bis(4-bromophenyl)-N^1,N^3,N^5,N^5-tetrakis(4-(hexyloxy) phenyl)benzene-1,3,5-triamine (4)

A mixture of compound 3 (1.00 g, 1.21 mmol), 1,4-dibromobenzene (2.85 g, 12.1 mmol), $Pd(OAc)_2$ (0.01 g, 0.06 mmol), DPPF (0.07 g, 0.13 mmol), and sodium *tert*-butoxide (0.35 g, 3.64 mmol) were heated in dry toluene at 110 °C under an inert N_2 atmosphere. After

12 h, the crude reaction mixture was treated with a saturated ammonium chloride solution and extracted with dichloromethane. The organic phase was washed with brine, dried over $MgSO_4$, and the solvent was evaporated under vacuum. The crude product was purified by column chromatography (silica gel, MC–hexane 1:2) to give 0.98 g (71%) of compound 4. ^{1}H NMR (300 MHz, $CDCl_3$) δ: 0.90 (m, 12H), 1.33–1.36 (m, 24H), 1.56 (m, 8H), 3.88 (m, 8H), 6.12 (s, 1H), 6.19 (s, 2H), 6.68–6.80(m, 12H), 6.91 (t, 8H), 7.16 (d, 4H); ^{13}C NMR (300 MHz, $CDCl_3$) δ: 14.5, 22.8, 25.9, 29.5, 31.80, 68.4, 113.2, 116.2, 125.4, 126.5, 126.9, 127.9, 132.3, 139.6, 140.3, 147.0, 148.6, 149.9, 155.2, 155.9.

2.4.5. 5′,5″-(4,4′-(5-(Bis(4-(hexyloxy)phenyl)amino)-1,3-phenylene)bis((4 (hexyloxy)phenyl)azanediyl)bis(4,1-phenylene)) di-2,2′-bithiophene-5-carbaldehyde (5)

A mixture of compound 4 (0.23, 0.20 mmol), (5′-(1,3-dioxolan-2-yl)-2,2′-bithiophen-5-yl)tributylstannane (0.32 g, 0.61 mmol), $Pd(PPh_3)_2Cl_2$ (0.02 g, 0.03 mmol), in 50 mL dry THF was refluxed overnight under N_2 atmosphere. The reaction was monitored by thin layer chromatography. After complete consumption of starting material, concentrated hydrochloric acid (0.5 mL) was added, the mixture was stirred at room temperature for 10 min and extracted with dichloromethane. The organic phase was washed with brine, dried over $MgSO_4$, and the solvent was evaporated under vacuum. The crude product was purified by column chromatography (silica gel, MC) to give 0.19 g (69%) of compound 5. ^{1}H NMR (300 MHz, $CDCl_3$) δ 0.82–1.01 (m, 12H), 1.26–1.55 (m, 24H), 1.68–1.79 (m, 8H), 3.83 (t, 4H), 3.90 (t, 4H), 6.25 (s, 1H), 628 (s, 2H), 6.69 (d, 4H), 6.77 (d, 4H), 6.91 (t, 8H), 6.97 (m, 5H), 7.04 (d, 2H), 7.20(d, 2H), 7.26–7.29 (m, 6H), 7.33 (d, 4H), 7.64 (d, 2H), 9.84 (s, 2H); ^{13}C NMR (300 MHz, $CDCl_3$) δ 13.8, 14.3, 17.7, 22.8, 25.9, 27.1, 28.0, 29.5, 31.8, 68.4, 111.1, 115.1, 115.3, 121.6, 122.9, 123.6, 125.9, 126.2, 126.4, 127.4, 133.7, 139.3, 140.3, 141.2, 146.6, 147.6, 148.1, 148.4, 150.0, 155.2, 156.1, 182.5.

2.4.6. (2E,2′E)-3,3′-(5′,5′′-(4,4′-(5-(Bis(4-(hexyloxy)phenyl)amino)-1,3-phenylene)bis((4-(hexyloxy)phenyl)azanediyl)bis(4,1-phenylene))bis(2,2′-bithiophene-5′,5-diyl))bis(2-cyanoacrylic acid) (DC5)

Compound 5 (0.07 mg, 0.05 mmol), dissolved in $CHCl_3$ (20 mL) and acetonitrile (20 mL), was condensed with 2-cyanoacetic acid (0.01 g, 0.12 mmol) in the presence of piperidine (0.01 mL, 0.12 mmol). The mixture was refluxed for 12 h. After cooling the solution, the organic layer was removed in vacuo. Dark red solid of DC5 was obtained by silica gel chromatography (MC/MeOH = 4:1); Yield was 78%. ^{1}H NMR (300 MHz, DMSO-d_6) δ 0.86–0.88 (m, 12H), 1.10–1.59 (m, 24H), 1.97(m, 8H), 3.79–3.86 (m, 8H), 5.98 (m, 3H), 6.78–7.02 (m, 18H), 7.38 (m, 12H), 7.68 (m, 4H), 8.08 (s, 2H); ^{13}C NMR (300 MHz, DMSO-d_6) δ 13.8, 14.3, 17.7, 22.8, 25.9, 27.1, 28.0, 29.5, 31.8, 68.4, 111.1, 115.1, 115.3, 121.6, 122.9, 123.6, 125.9, 126.2, 126.4, 127.4, 133.7, 139.3, 140.4, 141.2, 146.2, 147.3, 148.3, 148.5, 150.4, 155.7, 156.1, 163.5; UV–vis (THF, nm): λ_{max} (log ε) 440 (41700). PL (THF, nm): λ_{max} 645; MS (MALDI-TOF): Calcd. for $C_{90}H_{91}N_5O_8S_4$, 1498.97; found, 1498.62.

2.5. Fabrication and testing of DSSC

FTO glass plates (Pilkington) were cleaned in a detergent solution using an ultrasonic bath for 1 h, then rinsed with water and ethanol. The FTO glass plates were immersed in an aqueous solution of 40 mM $TiCl_4$ at 70 °C for 30 min and then washed with water and ethanol. The first TiO_2 layer with a thickness of 12 μm was prepared by screen-printing TiO_2 paste (Solaronix, 13 nm anatase), and the second scattering layer containing 400 nm sized anatase particles was deposited by screen printing. The TiO_2 electrodes were immersed into the dye solution (0.3 mM) in THF/EtOH (1:2) with DCA (40 mM) or HC-A1 (1 mM) and kept at room temperature overnight. Counter-electrodes were prepared by coating with a drop of H_2PtCl_6 solution (2 mg of Pt in 1 mL of ethanol) on an FTO plate. The dye-adsorbed TiO_2 electrode and Pt counter electrode were assembled in a sealed sandwich-type cell. One drop of electrolyte was then introduced into the cell, which was composed of 0.6 M 1,2-dimetyl-3-propyl imidazolium iodide, 0.05 M iodine, 0.1 M LiI, and 0.5 M *tert*-butylpyridine in acetonitrile. The electrolyte was introduced into the inter-electrode space from the counter electrode side through predrilled holes. The drilled holes were sealed with a microscope cover slide and Surlyn to avoid leakage of the electrolyte solution.

2.6. Photoelectrochemical measurements of DSSC

Photoelectrochemical data were measured using a 1000 W xenon light source (Oriel, 91193) that was focused to give 1000 W/m^2, the equivalent of one sun at AM 1.5G, at the surface of the test cell. The light intensity was adjusted with a Si solar cell that was double-checked with an NREL-calibrated Si solar cell (PV Measurement Inc.). The applied potential and measured cell current were measured using a Keithley model 2400 digital source meter. The current–voltage characteristics of the cell under these conditions were determined by biasing the cell externally and measuring the generated photocurrent. This process was fully automated using Wavemetrics software.

3. Results and discussion

The synthetic procedures of dual-channel (DC) dye containing triphenylamine is depicted in Scheme 1. DC aldehyde derivative was synthesized by the Stille coupling reaction, and the DC5 sensitizer was synthesized by the reaction of compound 5 with cyanoacetic acid in the presence of a piperidine catalyst.

Fig. 1 shows the absorption and emission spectra of the DC5 dye measured in THF solution; the photophysical properties are summarized in Table 1. In the UV–vis spectrum, the DC5 dye exhibited two main prominent bands, appearing at 350–400 and 400–500 nm, respectively. The former was ascribed to the localized aromatic π–π^* transition, and the latter was that of the charge-transfer character, which was from the donor part to the acceptor group. The absorption spectrum of the DC5 dye showed maximum absorption at 440 nm, which was 18 nm blue-shifted in contrast to D21L6 dye. But, the molar absorption coefficient (ε) of the DC5 dye (ε_{max} = 41,700 M^{-1} cm^{-1}) was much higher than that of D21L6 (ε_{max} = 27,700 M^{-1} cm^{-1}), indicating that the DC5 dye could have better light-harvesting ability. The dianchoring mode of DC5 dye was further confirmed by ATR-FTIR spectroscopy (Fig. 2). The C=O stretching band at 1730 cm^{-1} assigned to the carboxylic acid groups of free DC5 dye was found to have disappeared in the IR spectrum of DC5 dye adsorbed on TiO_2 film, indicating the involvement of both carboxylic acid groups in adsorption on the TiO_2 surface; this result is similar to the observations made by Heredia et al. [17] and Abbotto et al. [18]

The electrochemical properties were investigated by cyclic voltammetry (CV) to obtain the HOMO and LUMO levels of the DC5 dye. The cyclic voltammograms were obtained from a three-electrode cell in 0.1 M $TBAPF_6$ in CH_3CN at a scan rate of 50 mV s^{-1}, using a dye coated TiO_2 electrode as the working electrode, a Pt wire counter-electrode, and an Ag/AgCl (saturated KCl) reference electrode (+0.197 V vs. NHE) which was calibrated with ferrocene. All of the measured potentials were converted to the NHE scale. The band gap was estimated from the absorption edges of the UV–vis spectra and LUMO energy levels were derived from the HOMO energy levels and the band gap. HOMO values (0.94 V vs.

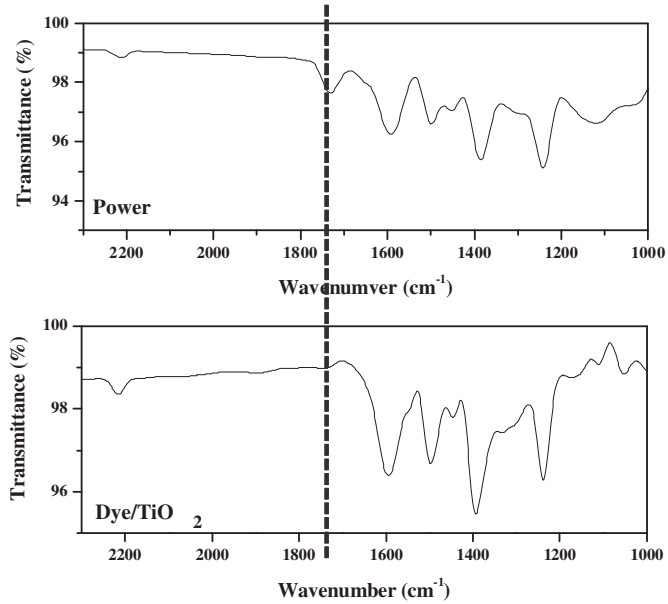

Fig. 2. ATR-FTIR spectra of DC5 dye.

NHE) were more positive than the I^-/I_3^- redox couple (0.4 V vs. NHE). Electron injection from the excited dyes to the conduction band of TiO_2 should be energetically favorable because of the more negative LUMO values (−1.32 V vs. NHE) compared to the conduction band edge energy level of the TiO_2 electrode [28].

Here, structural optimization of dual-channel (DC) dye was also done with a PBE exchange-correlation function using the Vienna ab initio simulation package (VASP). We summarize our results for the DFT and TD-DFT calculations. First, our optimization results indicate that the *cis* configuration is more stable than the *trans* configuration by 0.06 eV. Therefore, we can conclude that the DC5 dye predominantly adopt the *cis* configuration, and the TD-DFT calculations were performed for the configuration. The closest distances between the two *m*-phenylene units were 6.6 and 15.1 Å for the *cis* and *trans* configurations, respectively (Fig. S3). The ϕ angles were −10.2° and 47.1° for *cis* and *trans* configurations, respectively. Such an inter-planar conformation leads to intermolecular π−π stacking interactions between channels of DC5 dye adsorbed on the TiO_2 surface. It is well-known that the π−π stacking of the inter-planar molecules may facilitate the formation of detrimental excimeric species and lead to fluorescence quenching in the solid state [29].

In very good agreement with the experimental data shown in Fig. 1, we first find two absorption maxima. We were able to confirm that absorption peaks below 400 nm are not observed if only 40 transitions are examined. The major absorption appears at 488 nm, which is red-shifted by 48 nm with respect to the experimental data. Now, we delve into the nature of transitions responsible for the observed absorption maxima. Table S1 shows that six absorptions at 462, 465, 474, 490, 498, and 509 nm, which are responsible for the absorption peak at 488 nm, can be largely ascribed to five charge transfer transitions, i.e., HOMO 7 → LUMO+1, HOMO−6 → LUMO, HOMO−2 → LUMO+3, HOMO−1 → LUMO+2, and HOMO−1 → LUMO+3 transitions. (See Fig. 3 for the isodensity plots of the four molecular orbitals.) Note that the (HOMO−7, HOMO−6) are doubly degenerate, which is also true for (LUMO, LUMO+1) and (LUMO+2, LUMO+3).

To effectively suppress dye aggregation for DSSCs, in our previous study [30–35], coadsorbents such as DCA and HC-A1 were used. Both V_{oc} and J_{sc} were dramatically enhanced by the coadsorption of the multi-functional coadsorbent HC-A1 with the dye, due to the efficient retardation of charge recombination arising

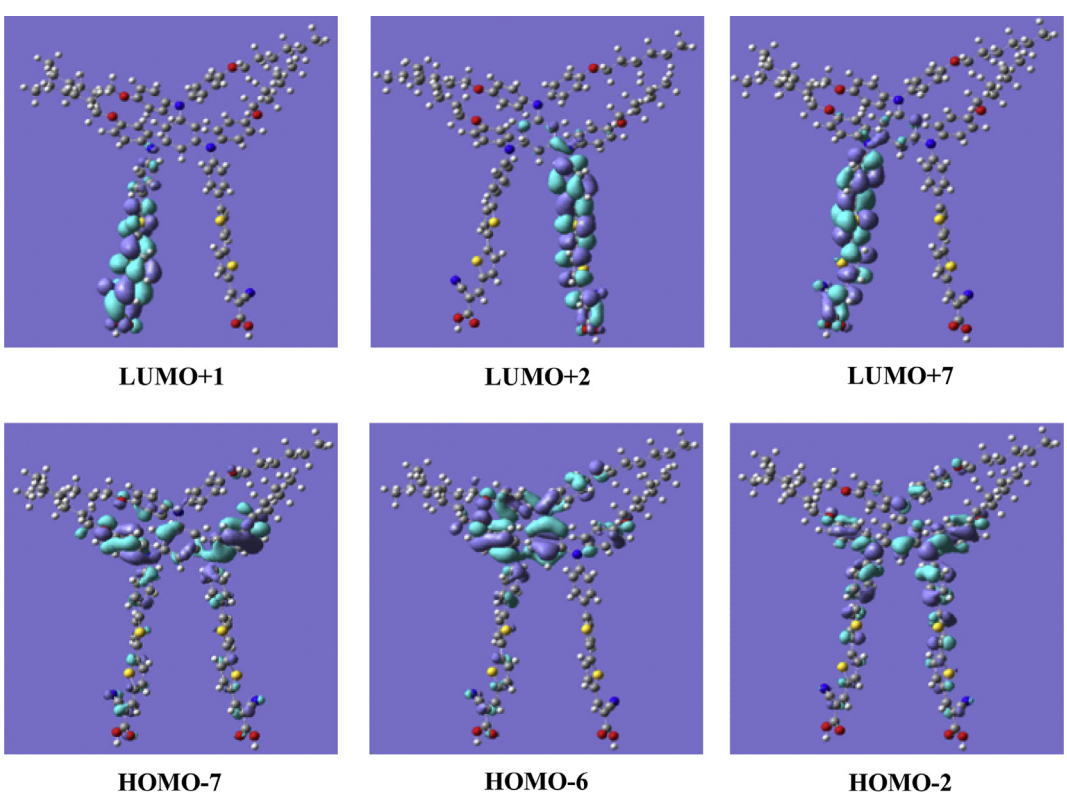

Fig. 3. Isodensity plots of the HOMO−7 (a), HOMO−6 (b), HOMO−2 (c), LUMO+1, (d), LUMO+2 (e) and LUMO+3 (f) of the DC5 dye.

from the prevention of π–π stacking, light-harvesting in shorter wavelength regions, and a hole conducting function through a redox cascade process [30]. Fig. 4 shows the spectra for the efficiency of conversion of an incident photon to current (IPCE) for the DSSCs with dye only and dye/coadsorbent, respectively. The onset wavelengths of the IPCE spectra for DSSCs based on DC5 were about 700 nm. For DSSCs based on DC5 and DC5/DCA, the IPCE spectra exhibit the sharp peak below 400 nm, which could correspond to the absorption of TiO_2 film [28]. The IPCE values of higher than 50% were observed in the range of 350–600 nm with a maximum value of 60% at 490 nm for the DSSC based on DC5 with HC-A1. The IPCE response of the DC5/HC-A1-sensitized DSSC was remarkably increased compared to that with DCA. We suggest that intermolecular π–π stacking between channels of DC5 dye adsorbed on the TiO_2 surface was effectively reduced by the incorporation of coadsorbents, resulting in the enhanced light harvesting.

The photovoltaic performances of the DC- and D21L6-sentsitized DSSCs are summarized in Table 2. Under standard global AM 1.5 solar conditions, the DC5 sensitized cell (without coadsorbents) gave a short circuit photocurrent density (J_{sc}) of 1.34 mA cm^{-2}, an open circuit voltage (V_{oc}) of 0.45 V, and a fill factor (*FF*) of 0.76, corresponding to an overall conversion efficiency (η) of 0.46% due to heavy aggregation. On the other hand, the DC1/DCA-sensitized DSSC, compared to the DC5-sensitized DSSC, J_{sc} increased from 1.34 to 5.70 mA cm^{-2}, 0.45–0.54 V for V_{oc}, and 0.46–2.41% for η. As shown in Fig. 4, J_{sc} increased in the same order as the integrated photocurrent from the IPCE spectrum. Also, the DC5/HC-A1-sensitized DSSC, compared to the DC5/DCA-sensitized DSSC, had an increased J_{sc} from 5.70 to 8.92 mA cm^{-2}, 0.54–0.69 V for V_{oc}, and 2.41–4.78% for η. It was observed that the coadsorption of either DCA or HC-A1 simultaneously improved J_{sc} and V_{oc}, but coadsorption with HC-A1 enhanced J_{sc} and V_{oc} more significantly than with DCA. The HC-A1 has multiple functions, such as the light-harvesting function as a short-wavelength light absorption dye molecule to increase J_{sc}, the prevention effect of the π–π stacking of organic dye to enhance V_{oc} by reducing the charge recombination [30–32]. On the other hand, the D21L6/DCA-sensitized DSSC gave a J_{sc} of 13.5 mA cm^{-2}, V_{oc} of 0.67 V, and a *FF* of 0.72, corresponding to η of 6.67%. These results indicate that the DC structure leads to heavier aggregation and charge recombination than the single D–π–A structured D21L6 due to intermolecular π–π stacking between adsorbed channels on the TiO_2 surface (Fig. 5).

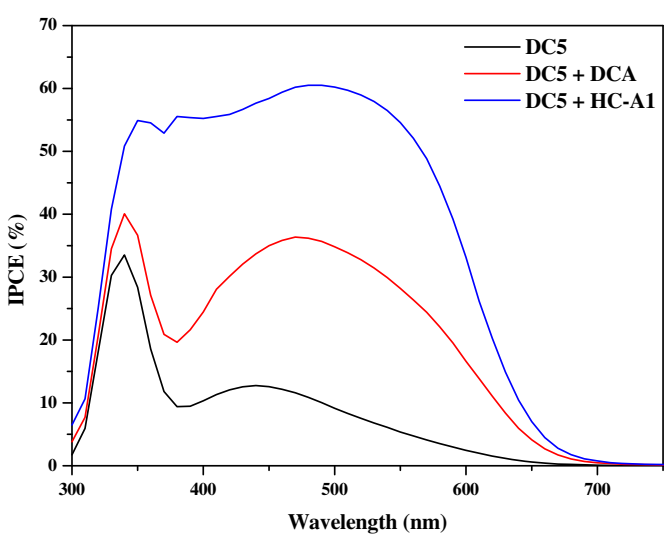

Fig. 4. Typical action spectra of incident photon-to-current conversion efficiencies (IPCE) obtained for nanocrystalline TiO_2 solar cells sensitized by DC5 dye.

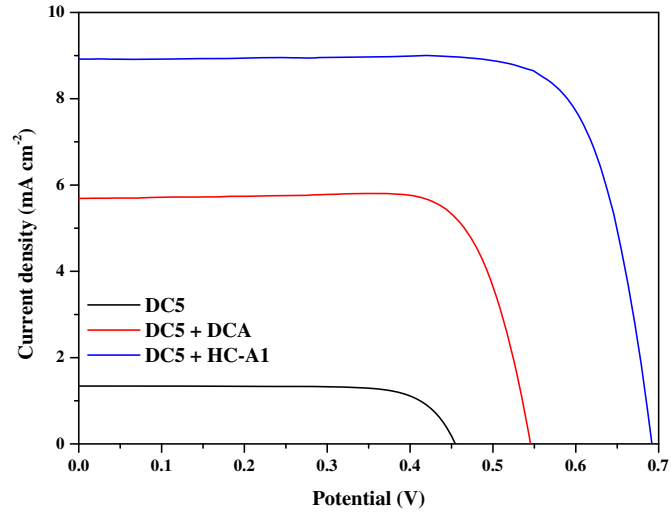

Fig. 5. Photocurrent-voltage characteristics of representative TiO_2 electrodes sensitized with DC5 dye.

To further characterize the open circuit voltage effect with respect to the coadsorbents used, we measured electrochemical impedance spectroscopy (EIS) under dark conditions. Their EIS parameters calculated from the equivalent circuit are summarized in Table 3. Typical Nyquist and Bode plots for the DSSCs based on the DC5 dye, DC5/DCA, and DC5/HC-A1 are shown in Fig. 6. The DC5/HC-A1-sensitized DSSC revealed relatively high charge transfer resistance compared with the dye only and DCA, while the frequency was apparently shifted to the lower frequency region. The maximum frequencies (ω_{max}) in the middle frequency region of the Bode plots of the DC5/HC-A1, DC5/DCA and DC5 sensitized DSSCs were 5.2, 10.1 and 144 Hz, respectively. Since ω_{max} is inversly associated with electron lifetime (τ), $\tau = 1/(2\pi f)$ [36], a decrease in ω_{max} indicates a reduced rate of the charge-recombination process of the DSSCs. The calculated τ values of DC/HC-A1-based device (8.69 ms) was slower than those of the DC only and DC/DCA-based devices (2.29 ms, 6.23 ms), which was consistent with the sequence of open circuit voltage values in the devices, and which might also be due to the significant increased in capacitance (C_μ) at the interface of the counter electrode/dye/electrolyte solution (Table 3). C_μ of DC/HC-A1-based device was enhanced due to the decrease electron loss by efficient prevention of charge recombination and π–π stacking. From the EIS results, it is clear that the charge recombination rate was the rate-determining step of the DSSC in terms of device performance, since the DC5-DSSCs with coadsorbents decreased the charge recombination rate and resulted in an improvement in device performance, in that order. From these results, we can conclude that charge recombination of the DSSCs with dye only is faster than that of the DSSCs with coadsorbents (DCA and HC-A1). This insulating molecular layer effectively inhibits back electron transfer from TiO_2 to I_3^- ions and results in a higher V_{oc}.

Table 3
Numerical values of the electrochemical impedance spectra for DSSCs based on DC5 dye.

Dye	Coadsorbent	R_{ct} (Ω)	C_μ (mF)	τ (ms)
DC5	–[a]	303.8	0.08	2.29
	DCA 40 mM[b]	64.5	0.97	6.23
	HC-A1 1 mM[c]	44.6	1.95	8.69

[a] Calculated from the EIS spectrum at a forward bias of ~0.45 V.
[b] Calculated from the EIS spectrum at a forward bias of ~0.55 V.
[c] Calculated from the EIS spectrum at a forward bias of ~0.7 V.

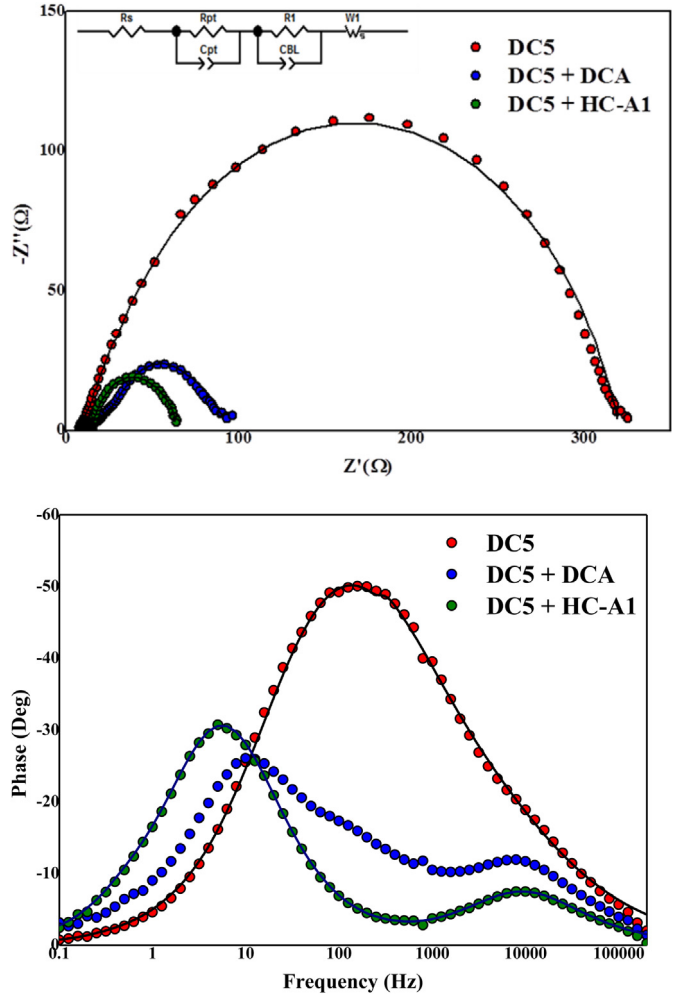

Fig. 6. Nyquist and Bode phase plots of electrochemical impedance spectra for the DSSC-based DC5 dye.

4. Conclusions

We successfully designed and synthesized dye based on a dual channel system to yield materials with interesting optical and electrochemical properties. The high molar absorption coefficient was favorable for the light-harvesting efficiency of DSSCs. The inter-planar DC5 dye had heavy aggregation and charge recombination due to strong intermolecular π–π stacking between channels adsorbed on the TiO_2 surface. The DC5/HC-A1-sensitized DSSC had a high V_{oc} than DC5- and DC5/DCA-sensitized DSSCs due to the prevention of aggregation and charge recombination. As a result, the solar cell based on the DC5 dye with HC-A1 showed better photovoltaic performance than solar cells based on DC5 with DCA, with a J_{sc} of 8.92 mA cm^{-2}, a V_{oc} of 0.69 V, and an *FF* of 0.77, corresponding to an overall conversion efficiency η of 4.78% under standard AM 1.5 irradiation.

Acknowledgments

This work was supported by the Human Resources Development program (No. 20124010203190) of the Korean Institute of Energy Technology Evaluation and Planning (KETEP) grant funded by the Korea Government Ministry of Trade, Industry and Energy. Prof. H. S. Kang gratefully acknowledges the computations performed using a supercomputer at the Korea Institute of Science and Technology Information (KSC-2013-C2-014).

Appendix A. Supplementary data

Supplementary data related to this article can be found at http://dx.doi.org/10.1016/j.dyepig.2013.06.014.

References

[1] Nazeeruddin MK, De Angelis F, Fantacci S, Selloni A, Viscardi G, Grätzel M, et al. Combined experimental and DFT-TDDFT computational study of photoelectrochemical cell ruthenium sensitizers. J Am Chem Soc 2005;127:16835–47.
[2] He H, Dubey M, Zhong Y, Shrestha M, Sykes AG. 2-(1-Acetyl-2-oxopropyl)-5,10,15,20-tetraphenylporphyrin and its transition-metal complexes. Eur J Inorg Chem 2011;25:3731–8.
[3] Mishra A, Fischer MKR, Bäuerle P. Metal-free organic dyes for dye-sensitized solar cells: from structure: property relationships to design rules. Angew Chem Int Ed Engl 2009;48:2474–99.
[4] Ning Z, Fu Y, Tian H. Improvement of dye-sensitized solar cells: what we know and what we need to know. Energy Environ Sci 2010;3:1170–81.
[5] Mao J, He N, Ning Z, Zhang Q, Hua J, Tian H, et al. Stable dyes containing double acceptors without COOH as anchors for highly efficient dye-sensitized solar cells. Angew Chem Int Ed Engl 2012;51:9873–6.
[6] Yen YS, Chou HH, Chen YC, Hsu CY, Lin JT. Recent developments in molecule-based organic materials for dye-sensitized solar cells. J Mater Chem 2012;22:8734–47.
[7] Seo KD, Lee MJ, Song HM, Kang HS, Kim HK. Novel D-π-A system based on zinc porphyrin dyes for dye-sensitized solar cells: synthesis, electrochemical, and photovoltaic properties. Dye Pigment 2012;94:143–9.
[8] Lee MJ, Seo KD, Song HM, Kang MS, Kang HS, Kim HK, et al. Novel D-π-A system based on zinc-porphyrin derivatives for highly efficient dye-sensitised solar cells. Tetrahedron Lett 2011;52:3879–82.
[9] Yella A, Lee HW, Diau EWG, Yeh CY, Zakeeruddin SM, Grätzel M, et al. Porphyrin-sensitized solar cells with cobalt (II/III)-based redox electrolyte exceed 12 percent efficiency. Science 2011;334:629–34.
[10] Hagberg DP, Marinado T, Karlsso KM, Nonomura K, Hagfeldt A, Sun L, et al. Tuning the HOMO and LUMO energy levels of organic chromophores for dye sensitized solar cells. J Org Chem 2007;72:9550–6.
[11] Baek NS, Yum JH, Zhang X, Kim HK, Nazeerudin MK, Grätzel M. Functionalized alkyne bridged dendron based chromophores for dye-sensitized solar cell applications. Energy Environ Sci 2009;2:1082–7.
[12] Seo KD, Song HM, De Angelis F, Nazeeruddin MK, Gräetzel M, Kim HK, et al. Coumarin dyes containing low-band-gap chromophores for dye-sensitised solar cells. Dye Pigment 2011;90:304–10.
[13] Seo KD, Choi IT, Park YG, Kang S, Lee JY, Kim HK. Novel D-A-π-A coumarin dyes containing low band-gap chromophores for dye-sensitised solar cells. Dye Pigment 2012;94:469–74.
[14] Wang ZS, Koumura N, Cui Y, Takahashi M, Sekiguchi H, Hara K, et al. Hexylthiophene-functionalized carbazole dyes for efficient molecular photovoltaics: tuning of solar-cell performance by structural modification. Chem Mater 2008;20:3993–4003.
[15] Ning Z, Zhang Q, Wu W, Pei H, Liu B, Tian H. Starburst triarylamine based dyes for efficient dye-sensitized solar cells. J Org Chem 2008;73:3791–7.
[16] Lee DH, Lee MJ, De Angelis F, Nazeeruddin MK, Gräetzel M, Kim HK, et al. Organic dyes incorporating low-band-gap chromophores based on π-extended benzothiadiazole for dye-sensitized solar cells. Dye Pigment 2011;91:192–8.
[17] Heredia D, Natera J, Gervaldo M, Otero L, Fungo F, Wong KT, et al. Spirobifluorene-bridged donor/acceptor dye for organic dye-sensitized solar cells. Org Lett 2010;12:12–5.
[18] Abbotto A, Manfredi N, Marinzi C, De Angelis F, Nazeeruddin MK, Grätzel M, et al. Di-branched di-anchoring organic dyes for dye-sensitized solar cells. Energy Environ Sci 2009;2:1094–101.
[19] Abbotto A, Leandri V, Manfredi N, De Angelis F, Nazeeruddin MK, Grätzel M, et al. Bis-donor–bis-acceptor tribranched organic sensitizers for dye-sensitized solar cells. Eur J Org Chem 2011:6195–205.
[20] Ren X, Jiang S, Cha M, Zhou G, Wang ZS. Thiophene-bridged double D-π-A dye for efficient dye-sensitized solar cell. Chem Mater 2012;24:3493–9.
[21] Sirohia R, Kim DH, Yu SC, Lee SH. Novel di-anchoring dye for DSSC by bridging of two mono anchoring dye molecules: a conformational approach to reduce aggregation. Dye Pigment 2012;92:1132–7.
[22] Li Q, Shi J, Li H, Li S, Zhong C, Li Z, et al. Novel pyrrole-based dyes for dye-sensitized solar cells: from rod-shape to "H" type. J Mater Chem 2012;22:6689–96.
[23] Wang E, Meng Q, Wang C, Li L, Li H, Hu W. Syntheses and properties of cyano and dicyanovinyl-substituted oligomers as organic semiconductors. Synth Met 2009;159:1298–301.
[24] Yum JH, Hagberg DP, Moon SJ, Karlsson KM, Marinado T, Sun L, et al. A light-resistant organic sensitizer for solar-cell applications. Angew Chem Int Ed Engl 2009;48:1576–80.
[25] Kresse G, Hafner J. Ab initio molecular dynamics for liquid metals. Phys Rev B 1993;47:558–61.
[26] Kresse G, Furthmuller J. Efficient iterative schemes for ab initio total-energy calculations using a plane-wave basis set. Phys Rev B 1996;54:11169–86.

[27] Frisch MJ, Trucks GW, Schlegel HB, Scuseria GE, Robb MA, Cheeseman JR, et al. Gaussian03, revision B.05. Pittsburgh PA: Gaussian, Inc.; 2003.
[28] Hagfeldt A, Grätzel M. Light-induced redox reactions in nanocrystalline systems. Chem Rev 1995;95:49–68.
[29] Tong H, Hong YN, Dong YQ, Ren Y, Häussler M, Tang BZ, et al. Color-tunable, aggregation-induced emission of a butterfly-shaped molecule comprising a pyran skeleton and two cholesteryl wings. J Phys Chem B 2007;111:2000–7.
[30] Song BJ, Song HM, Choi IT, Kim SK, Seo KD, Kim HK, et al. A desirable hole-conducting coadsorbent for highly efficient dye-sensitized solar cells through an organic redox cascade strategy. Chem Eur J 2011;17:11115–21.
[31] Ju MJ, Kim JC, Choi HJ, Choi IT, Kim SG, Kim HK, et al. N-doped graphene nanoplatelets as superior metal-free counter electrodes for organic dye-sensitized solar cells. ACS Nano 2013;7:5243–50.
[32] Choi IT, Ju MJ, Kang SH, Kang MS, You BS, Kim HK, et al. Structural effect of carbazole-based coadsorbents on the photovoltaic performance of organic dye-sensitized solar cells. J Mater Chem A 2013. http://dx.doi.org/10.1039/C3TA11508A.
[33] Kang MS, Kang SH, Kim SG, Choi IT, Ryu JH, Kim HK, et al. Novel D–π–A structured Zn(II)-porphyrin dyes containing a bis(3,3-dimethylfluorenyl)amine moiety for dye-sensitised solar cells. Chem Commun 2012;48:9349–51.
[34] Song HM, Seo KD, Kang MS, Choi IT, Kim SK, Kim HK, et al. A simple triaryl amine-based dual functioned co-adsorbent for highly efficient dye-sensitized solar cells. J Mater Chem 2012;22:3786–94.
[35] Kang SH, Choi IT, Kang MS, Eom YK, Kang HS, Kim HK, et al. Novel D–π–A structured porphyrin dyes with diphenylamine derived electron-donating substituents for highly efficient dye-sensitized solar cells. J Mater Chem A 2013;1:3977–82.
[36] Kern R, Sastrawan R, Ferber J, Stangl R, Luther J. Modeling and interpretation of electrical impedance spectra of dye solar cells operated under open-circuit conditions. Electrochim Acta 2002;47:4213–25.